The Astrophysical Journal, 854:127 (12pp), 2018 February 20 https://doi.org/10.3847/1538-4357/aaa8e2

Nonlinear Effects in Three-minute Oscillations of the Solar Chromosphere. II. Measurement of Nonlinearity Parameters at Different Atmospheric Levels

Jongchul Chae[1], Kyuhyoun Cho[1], Donguk Song[2], and Yuri E. Litvinenko[3]
[1] Astronomy Program, Department of Physics and Astronomy, Seoul National University, Seoul 08826, Republic of Korea
[2] National Astronomical Observatory of Japan, National Institutes of Natural Sciences, 2-21-1 Osawa, Mitaka, Tokyo 181-8588, Japan
[3] Department of Mathematics, University of Waikato, P. B. 3105, Hamilton 3240, New Zealand
Received 2017 November 19; revised 2018 January 2; accepted 2018 January 16; published 2018 February 20

Abstract

Recent theoretical studies suggest that the nonlinearity of three-minute velocity oscillations at each atmospheric level can be quantified by the two independent parameters—the steepening parameter and the velocity amplitude parameter. For the first time, we measured these two parameters at different atmospheric levels by analyzing a set of spectral lines formed at different heights of sunspots ranging from the temperature minimum to the transition region. The spectral data were taken by the Fast Imaging Solar Spectrograph of the Goode Solar Telescope, and by the Interface Region Imaging Spectrograph. As a result, from the wavelet power spectra of the velocity oscillations at different heights, we clearly identified the growth of the second harmonic oscillations associated with the steepening of the velocity oscillation, indicating that higher-frequency oscillations of periods of 1.2 to 1.5 minutes originate from the nonlinearity of the three-minute oscillations in the upper chromosphere. We also found that the variation of the measured nonlinearity parameters is consistent with the theoretical expectation that the nonlinearity of the three-minute oscillations increases with height, and shock waves form in the upper chromosphere. There are, however, discrepancies as well between theory and observations, suggesting the need to improve both theory and the measurement technique.

Key words: hydrodynamics – Sun: atmosphere – Sun: chromosphere – Sun: oscillations – waves

1. Introduction

Three-minute oscillations of velocity dominate the dynamics of a quiescent sunspot chromosphere (Beckers & Schultz 1972; Lites & Thomas 1985). They are the fundamental oscillations of a gravitationally stratified medium that are excited by various types of driving at the lower boundary, having a frequency ω slightly above the acoustic cutoff frequency ω_0. (Lamb 1909; Fleck & Schmitz 1991; Kalkofen et al. 1994). The three-minute oscillations in fact represent propagating long-wavelength acoustic (slow magnetoacoustic) waves that are highly dispersive (see, e.g., Kalkofen et al. 1994; Chae & Goode 2015; Chae & Litvinenko 2017). They have group speeds much lower than, and phase speeds much higher than, the sound speed, hence they look similar to standing waves, unlike short-wavelength acoustic waves that are non-dispersive.

Observations have indicated that the three-minute oscillations become nonlinear in the upper atmosphere. In fact, upward-propagating shock waves with periods of several minutes have been often detected in the upper chromosphere and the transition region (Hansteen et al. 2006; De Pontieu et al. 2007; Rouppe van der Voort & de la Cruz Rodriguez 2013; Chae et al. 2014; Tian et al. 2014). The detected signature of the arrival of a shock wave was the so-called *N*-pattern of velocity pattern characterized by a sudden switch from a fast downward motion to a fast upward motion, and the subsequent gradual drift of the velocity to the zero-velocity and then to the fast downward motion. In addition, Felipe et al. (2010) found that the phase difference of the three-minute oscillations between two different heights in the upper chromosphere is not compatible with the propagation of linear waves, indicating that the nonlinearity plays a role there.

The first attempt to analytically describe the nonlinear propagation of the dispersive long waves, i.e., the three-minute oscillations, was done by Litvinenko & Chae (2017). They noted that the wave-steepening results from the growth of the second harmonic and higher-order harmonics that are generated by the nonlinear terms in the wave equation. When the fundamental oscillation of velocity has the frequency ω, the quadratic terms of velocity in the wave equations yield the second harmonic frequency 2ω, and the higher-order terms, the higher harmonic frequencies 3ω, 4ω, and so on. Litvinenko & Chae (2017) obtained an approximate nonlinear wave solution for velocity that consists of the fundamental term and the second harmonic term, and suggested that the second harmonic signal should be detectable in an upper chromosphere.

Subsequently, Chae & Litvinenko (2017, Paper I hereafter) obtained a new nonlinear wave solution of an implicit form that can be used to model the steepening of the velocity profile at different heights in the three-minute oscillations. As a result of this solution, a theoretical relationship was established between two independent measurable parameters: one related to the amplitude-frequency product of the fundamental oscillation, and the other related to the ratio of the second harmonic to the fundamental one. Moreover, for the first time, Paper I detected the second harmonic signal in the velocity profile from the spectral analysis of the Na D_2 line and the Hα line.

This work is a continuation of Paper I. We aim to systematically investigate the nonlinearity of the three-minute oscillations at different atmospheric levels of sunspots. For this, based on the results of Paper I, we first describe the nonlinear analytical model of the velocity oscillation together with the two independent nonlinearity parameters: the steepening parameter and the oscillation amplitude parameter. We infer velocity oscillations at different atmospheric levels by analyzing the spectral data of seven spectral lines formed at different

heights ranging from the temperature minimum to the transition. The two parameters are determined by fitting the velocity oscillations with the nonlinear model. The empirically determined values of the model parameters are then compared with the theoretical relationship obtained in Paper I.

2. Nonlinear Model of Velocity Oscillation

Here, we present the model of the velocity profile based on Paper I. It is well-known that as a result of the steepening, a wave profile eventually has a sawtooth shape. By adopting the form of the implicit solution obtained for a nonlinear acoustic wave in a uniform medium (Lighthill 1978), Paper I proposed the equation of the form

$$v(t, z) = v_1(z)\sin\left(\omega t - \phi(z) + S(z)\frac{v}{v_1(z)}\right) \quad (1)$$

for the description of the velocity profile $v(t, z)$ of a nonlinear wave at a fixed position z. This specific equation is characterized by the four parameters: angular frequency ω, velocity amplitude v_1, phase ϕ, and steepening parameter S.[4] From a theoretician's point of view, these parameters are determined as functions of height z in the atmosphere. Paper I presented the expressions $\phi(z)$, $S(z)$ and $v_1(z)$ at heights of an isothermal atmosphere where $S(z) \leqslant 1$.

From an observer's point of view, the parameters are treated as free parameters to be determined from the observed velocity profile $v(t)$. In this approach, $S > 1$ is allowed. Note that if S is not zero, Equation (1) does not provide an explicit expression of v, but has to be solved for v. With $\theta \equiv \omega t - \phi$, and $x \equiv v/v_1$, Equation (1) can be reduced to an equivalent equation $f(x) = 0$ for $|x| \leqslant 1$, with $f(x)$ defined by

$$f(x) \equiv x - \sin(Sx + \theta). \quad (2)$$

Since $f(-1) \leqslant 0$ and $f(1) \geqslant 0$ for any pair of S and θ, the equation $f(x)$ should have at least one solution in the interval $[-1, 1]$. Moreover, we have $f(0) = -\sin(\theta)$. Therefore, if $\theta > 0$ then there is at least one solution in the interval $(0, 1]$ and if $\theta < 0$ then there is at least one solution in the interval $[-1, 0)$. If $0 \leqslant S \leqslant 1$, the function $f(x)$ is a monotonically increasing function, so the equation $f(x) = 0$ has one and only one solution in the interval $[-1, 1]$. For $S > 1$, $f(x)$ may have more than one solution for small $|\theta_1|$, where $\theta_1 \equiv \theta - 2\pi n$ for n is the integer closest to $\theta/(2\pi)$.

For physical application, we have to choose only one solution for each set of S and θ_1. We choose the positive one in the interval $(0, 1]$ if $\theta_1 > 0$, and 0 if $\theta_1 = 0$, the negative one in the interval $[-1, 0)$, irrespective of whether the equation $f(x)$ has a single solution or three solutions. This choice allows us to reproduce a jump in x between $\theta_1 = -\delta$ and $\theta_1 = +\delta$ for a small value, δ. The solution is numerically determined with the bisection method.

Figure 1 illustrates the velocity profiles in three different cases of S. Generally speaking, the S of an upwardly propagating wave increases with the height of the solar atmosphere because velocity amplitude v_1 increases with height z to compensate for the decrease of density. As S increases, the profile deviates from the sinusoidal profile, making the rise more rapid, and the descent slower, hence resulting in the steepened profile. The steepening is clearly noticeable when $S = 0.5$. Nevertheless, as long as $S < 1$, the velocity profile is continuous all times. At the height where $S = 1$, discontinuities appears in the velocity profile. This corresponds to the wave-breaking or the formation of shock waves. At the height where $S > 1$, the velocity profile has a jump at $t = 0$, representing a shock wave.

Because of the periodicity, the steepened velocity profile may be written as a Fourier series:

$$v(t) = \sum_{n=1}^{\infty} A_n \sin(n\theta), \quad (3)$$

where the amplitude A_n can be numerically calculated using the expression

$$A_n = \frac{1}{\pi}\int_{-\pi}^{\pi} v(\theta)\sin(n\theta)d\theta. \quad (4)$$

Figure 2 shows the plots of A_n for different values of n and their ratios as the functions S. We confirm from the figure that the steepening is due to the growth of the second harmonic, the third harmonic, and higher harmonics resulting from the nonlinear development. The most noteworthy is the linear growth of the amplitude ratio of the second harmonic to the fundamental one A_2/A_1 as S increases from zero. This means that the detection of the second harmonic can be used as observational evidence of the nonlinearity of the oscillations. Note that $A_2/A_1 \approx S/2$ for $S \ll 1$. When wave-breaking occurs, we have $S = 1$ and $A_2/A_1 \approx 0.42$. In the limit of the extreme nonlinearity with $S \gg 1$, we have $A_2/A_1 \approx 1/2$ and $A_3/A_1 \approx 1/3$.

The amplitude-frequency product $v_1\omega$ is another independent measure of the steepness of the velocity profile. It measures the time derivative of velocity at a point. Paper I defined its dimensionless form X by

$$X \equiv \frac{v_1\omega}{c_0\omega_0}, \quad (5)$$

with the local sound speed c_0 and local acoustic cutoff frequency ω_0. Note that the product $c_0\omega_0$ is equal to $\gamma g/2$, depending only on specific heat ratio γ and gravitational acceleration g, not on local temperature. Assuming the vertical propagation of adiabatic waves in the solar atmosphere, we may choose the constant values, $\gamma = 1.67$ and $g = 27{,}400\,\mathrm{cm\,s^{-2}}$, so the value of X is fully determined by the product $v_1\omega$ only.

We work with the two parameters X and S to understand the nonlinear development of acoustic waves in the solar atmosphere. From an observer's point of view, X and S are independently determined from observations. The fitting of the observed velocity profile $v_{\rm obs}$ by the model v in Equation (1) yields the independent parameters $v_1\omega$ and S. Note that for the model fitting, v should be known as a function of t for the given model parameters ω, ϕ, S, and v_1. We have carried out the constrained model fitting to the data using the Interactive Data Language program mpcurvefit.pro in the Solar software that implements the Levenberg–Marquardt least square method.

From a theoretician's point of view, X and S should be positively correlated to each other. As a matter of fact, Paper I derived the theoretical relationship between X and S for a

[4] The parameter S introduced here is identical to the parameter a introduced by Litvinenko & Chae (2017) and corresponds to twice the parameter R_2 introduced in Paper I.

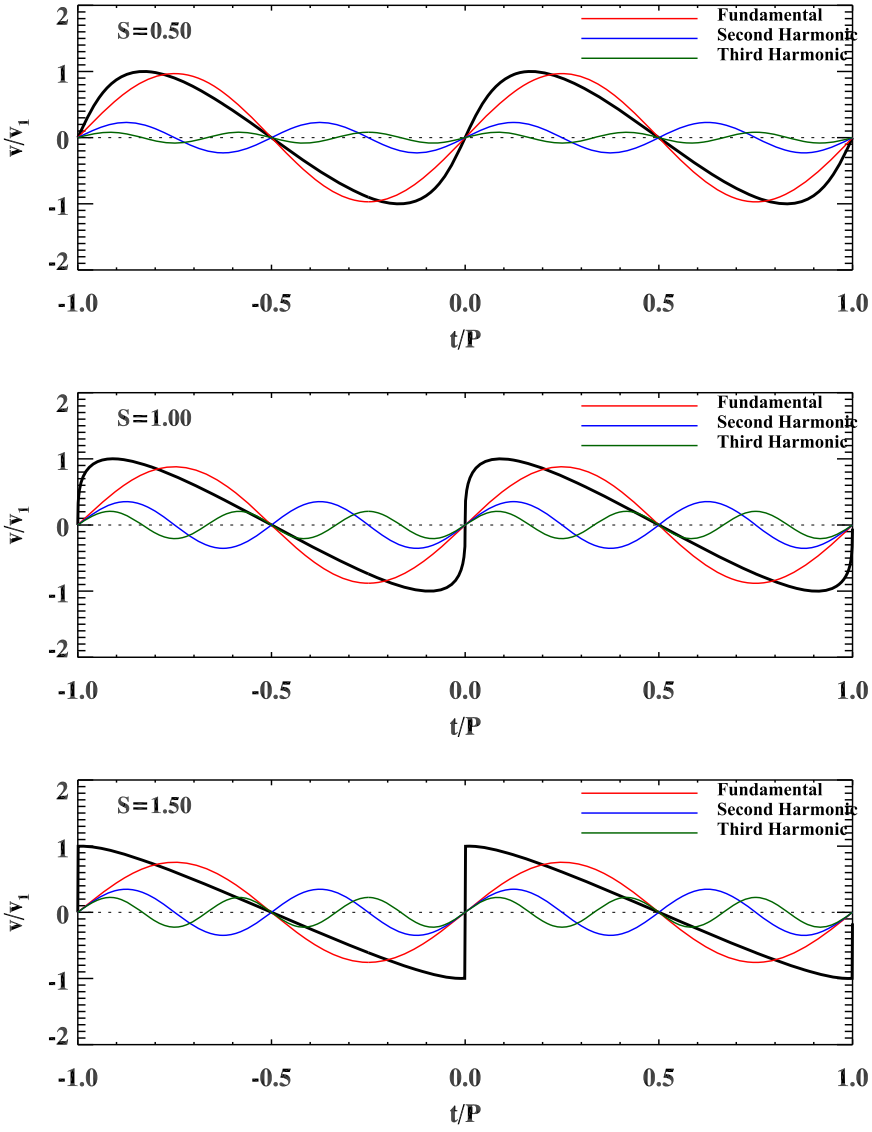

Figure 1. Velocity profiles in the three different cases of S.

propagating wave in an atmosphere. A non-negative parameter $b(z)$ as a function of height z was introduced to relate $S(z)$ to $X(z)$:

$$S(z) = X(z)b(z). \tag{6}$$

Specifically, in an isothermal atmosphere with pressure scale height H_p, $X(z)$ exponentially increases with height,

$$X(z) = X_0 e^{\frac{z}{H_v}}, \tag{7}$$

with velocity scale height $H_v \equiv 2H_p$. Note that $b(z)$ depends on the frequency of waves ω. The solution obtained for the long waves of $\omega \simeq \omega_0$ in Paper I is approximately given by

$$b(z) \approx 1 - \left(\cos\frac{\sqrt{3}z}{H_v} + \frac{1}{\sqrt{3}}\sin\frac{\sqrt{3}z}{H_v}\right)e^{-\frac{z}{H_v}}, \tag{8}$$

which increases from zero at $z = 0$, reaches a peak of 1.16 at $z = 1.81H_v$, decreases back, and approaches an asymptotic value of 1.0 at $z \gg H_v$. The solution is physically valid up to the shock formation height $z_{\rm wb}$, where S becomes equal to 1, and it follows $X(z_{\rm wb})\ b(z_{\rm wb}) = 1$. In the specific case of $X_0 = 0.01$, we obtain $z_{\rm wb} \approx 4.6H_v$. If we choose, for example, $H_p = 150$ km, we have $z_{\rm wb} = 1380$ km.

3. Data and Analysis

We measure the velocity oscillations at different layers of the sunspot atmosphere by analyzing the spectral data of several spectra lines. The velocity oscillations in the temperature minimum are inferred from the Fe I λ5434 absorption line; those in the low/middle chromosphere, from the Na I λ5890 (D_2) absorption line; those in the middle/upper chromosphere, from the Ca II λ8542 absorption line and the Hα absorption line; those in the upper chromosphere, from the Mg II λ2796 emission line; those in the low transition region from the C II λ1336 emission line; and those in the middle transition region, from the Si IV λ1394 emission line. Note that we assume that the measured Doppler velocities can be identified with the vertical velocities since all the observed regions were not far from the disk center.

Table 1 summarizes the observations used in the present study. The spectral data of the four strong absorption lines—the Fe I λ5434 line, the Na I D_2 line, the Ca II λ8542 line, and the Hα line

Table 1
Summary of the Observations Used in the Present Study

Instr.	Sp. lines	Date	Dura.	Cad.	AR	Location	References
FISS	Ca II λ8542 Hα	2014 Jun 03	68 minutes	20 s	12078	(134″, −318″)	Chae et al. (2015)
FISS	Fe I λ5434 Na I D_2	2015 Jun 16	38 minutes	16 s	12367	(−186″, −333″)	Chae et al. (2017)
IRIS	Mg II λ2796 C II λ1336 Si IV λ1394	2013 Sep 02	79 minutes	3 s	11836	(99″, 58″)	Tian et al. (2014)

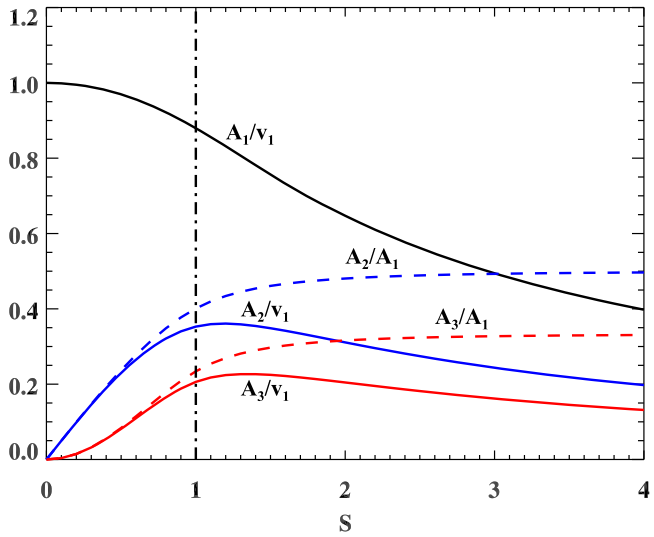

Figure 2. Normalized amplitudes of the fundamental (black solid curve), the second harmonic (blue solid curve), and the third harmonic (red solid curve), and the amplitude ratios of the second harmonic (blue dashed curve) and the third harmonic (red dashed curve) to the fundamental harmonic, calculated as functions of S.

were taken by the Fast Imaging Solar Spectrograph (FISS, Chae et al. 2013a) of the Goode Solar Telescope at Big Bear Solar Observatory. The Ca II line and Hα line spectra used for the present study were taken simultaneously at different points inside a pore observed on 2014 June 3 for 68 minutes at the cadence of 20 s. The details of the data and analysis were described by Chae et al. (2015). The Fe I line and Na I D_2 line spectra were taken simultaneously at different points inside a sunspot umbra observed on 2015 June 16 for 38 minutes at the cadence of 16 s. A detailed description of the data and the analysis can be found in Chae et al. (2017).

We infer the Doppler velocity from the core of each absorption line profile $I(\lambda)$ using the so-called lambdameter method (e.g., Deubner et al. 1996; Chae et al. 2013b). A "lambdameter" refers to a horizontal bar of length $2\Delta\lambda$ put on the $\lambda - I$ plane (See Figure 3). The lambdameter method determines λ_m, satisfying $I(\lambda_m - \Delta\lambda) = I(\lambda_m + \Delta\lambda)$ for a given $\Delta\lambda$. It is one of the methods to determine the Doppler velocity from a line profile. One advantage of this method over the other methods is that for a strong absorption line, one can choose different values of $\Delta\lambda$ to determine Doppler velocity at different heights. In the present study, we are mainly interested in the velocity at the height where the core of the line is formed, so we choose the value of $\Delta\lambda$ to make the lambdameter fit the core. We have chosen 0.05 Å for the Fe I line, 0.07 Å for the Na I D_2 line spectra, and 0.08 Å for the Ca II line, and 0.2 Å for the Hα line. The method is not sensitive to the specific value of $\Delta\lambda$, as far as the lambdameter fits the core part. The lambdameter method applied to the these lines is illustrated in Figure 3.

We define the Doppler velocity v by the formula

$$v = -\frac{\langle\lambda_m\rangle - \lambda_m}{\lambda_0}c, \tag{9}$$

where c is the speed of light, λ_0 is the laboratory wavelength of the line, and $\langle\lambda_m\rangle$ is the mean of all the values of λ_m of the line in each observation. With this formula, the velocity reference is set to the ensemble average of the line-forming region. The exact definition of this reference is not critical in the present study since we are interested in the velocity oscillations. Note that the velocity associated with the blueshift is defined to be positive, which corresponds to the upward motion in the solar atmosphere.

The spectral data of the three emission lines—the Mg II λ2796 line, the C II λ1336 line, and the Si IV λ1394 line were taken by the Interface Region Imaging Spectrograph (IRIS; De Pontieu et al. 2014). These lines are thought to be formed at the regions of temperature $10^{4.0}$ K, $10^{4.4}$ K, and $10^{4.9}$ K, representing the upper chromosphere, the lower transition region, and the middle transition region, respectively. We use the same data that were used by Tian et al. (2014). This set of data was taken by fixing the slit at the center of a sunspot with the cadence of 3 s. Because of the short exposure, the data are noisy. So we integrate every five exposures at the cost of degrading the cadence to 15 s. Moreover, for a regular profile shape, the data are smoothed over wavelength with a Gaussian smoothing function with a standard deviation equal to the spectral sampling. We have applied the lambdameter method to the processed spectral profiles, with $\Delta\lambda$ being set to 0.08Å in the Mg II line, 0.05Å in the C II line, and 0.05 Å in the Si IV line. With these values, the method makes use of the core part while the commonly used method of Gaussian profile fitting uses the whole line profile. The two methods yield different values when the line profile deviates too much from a Gaussian profile.

Figure 4 gives an illustration of the lambdameter method applied to the emission lines recorded by IRIS.

The time series of velocity at every point is analyzed with the program package of the wavelet transform developed by Torrence & Compo (1998). The Morlet wavelet transform is used to filter the data and to obtain the power spectrum as a function of both period and time. To remove the noise and the low-frequency pattern, a wavelet filter has been applied to each set of velocity data to pass the Fourier components with periods

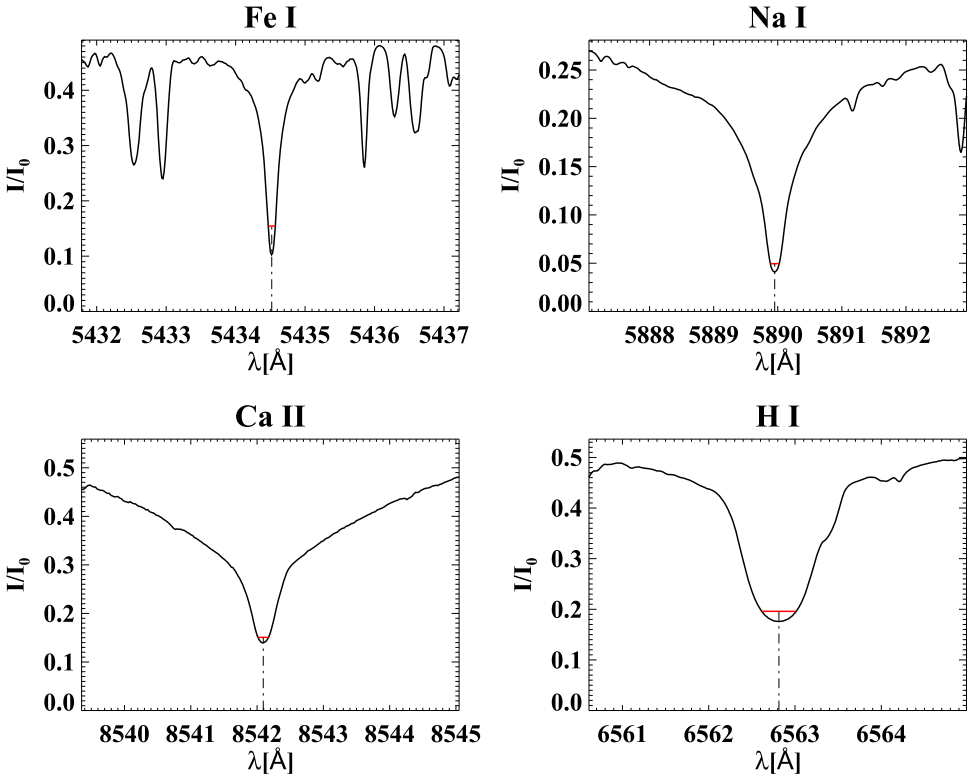

Figure 3. Illustration of the lambdameter method applied to the absorption line profiles recorded by the FISS at points inside sunspot umbrae. The small horizontal bars indicate the "lambdameter" used to infer the Doppler velocity from the cores of the lines. Each profile has been normalized by the mean continuum intensity I_0 outside sunspots.

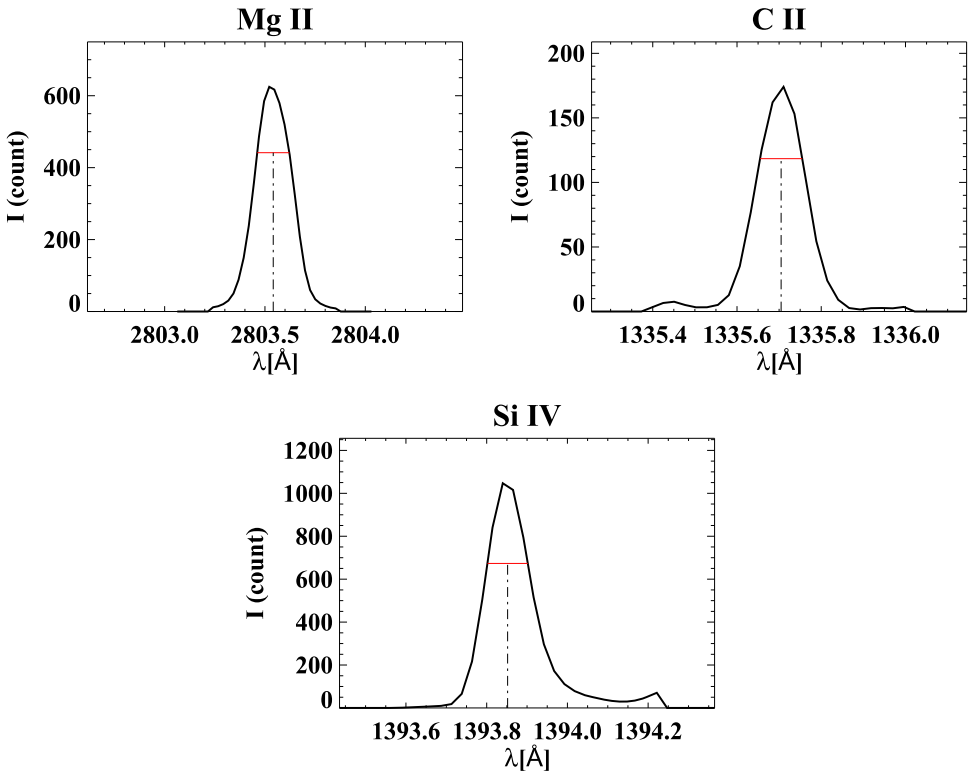

Figure 4. Illustration of the lambdameter method applied to the emission line profiles recorded by the IRIS at points inside sunspot umbrae. The small horizontal bars indicate the "lambdameter" used to infer the Doppler velocity from the cores of the lines.

from 0.5 to 4 minutes. In the Fe I line, the lower cutoff period is elevated to 1 minute to suppress the instrumental noise relevant to the imperfect operation of the spectrograph. The noise has a standard deviation of $0.01\,\mathrm{km\,s^{-1}}$, and a significant noisy contribution to the power spectrum of the Fe I velocity data in the period range from 0.5 to 1 minute. The velocity data

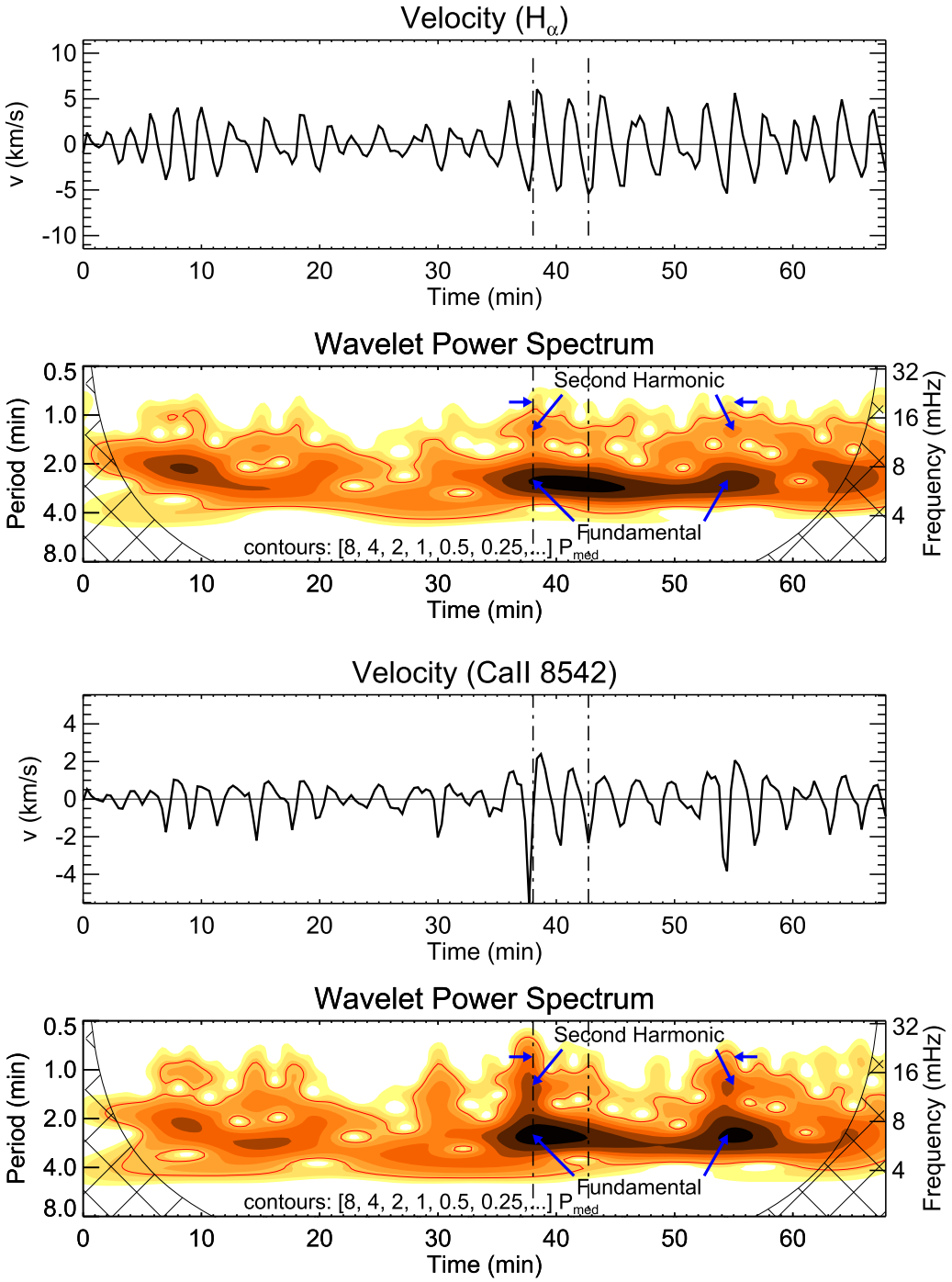

Figure 5. Top: time series of velocity and its wavelet power spectrum inferred from the Hα line at a fixed point inside a sunspot. The red contours are the significance level at the 95% confidence. The two vertical dotted–dashed lines indicate the temporal span of the data used as an example of the model fit. Each small horizontal arrow indicates the expected occurrence time and period of the third harmonic. Bottom: same as the top panel, but from the Ca II line. These two sets of velocity data were taken simultaneously from the same point.

inferred from the other lines have oscillation amplitudes much larger than 0.1 km s^{-1}, so the instrumental noise is negligible.

4. Results

4.1. The Second Harmonics

Figures 5–7 present some examples of velocity profiles and their wavelet power spectra obtained from the four absorption lines, and the three emission lines. They confirm that the three-minute oscillations prevail throughout the chromosphere and transition region from the formation height of the Fe I line to that of the Si IV line (e.g., Felipe et al. 2010; Tian et al. 2014; Chae et al. 2017). Moreover, we find from the figures that three-minute oscillations occur as discrete packets with a duration of 10 to 20 minutes, in agreement with previous studies (Kentischer & Mattig 1995; Christopoulou et al. 2003; Chae et al. 2017).

Figure 5 presents an example of the three-minute oscillations in the middle/upper chromosphere seen though the Hα line and the Ca II line. Note that the two sets of velocity data were

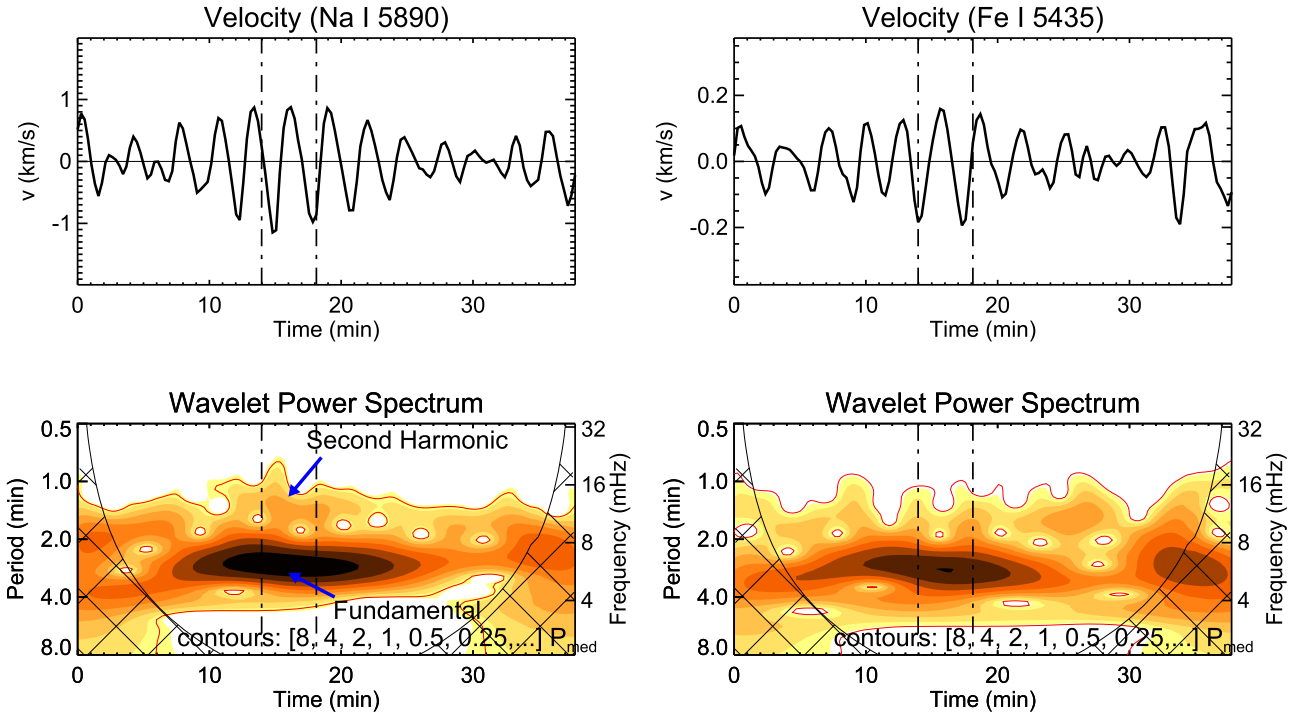

Figure 6. Left: time series of the Na I D_2 line Doppler velocity (top) and its wavelet power spectrum (bottom) at a fixed point inside a sunspot. Positive velocity values correspond to upward motion. Right: the same, but from the Fe I line. These two sets of velocity data were taken simultaneously from the same point.

taken simultaneously at the same point. The second harmonics are clearly identified in both the wavelet power spectra. They are characterized by a series of power enhancements at the frequencies twice those of the fundamental oscillations at the times of strong oscillation power and steep velocity rise. The occurrence of the second harmonics is evidence that the three-minute oscillations become significantly nonlinear at the formation heights of the Ca II 8542 line and the Hα line.

We compare the velocity variation at the same point between the two lines. We first note that there is no noticeable difference in the oscillation phase between them. This suggests that the formation heights of the two lines may not differ much from each other, which is in agreement with the result of Chae et al. (2013b) obtained for quiet regions. Despite the proximity of the formation heights, the velocity variations of the two lines are not similar in a couple of ways. First, the rms velocity of the Ca II line is 1.0 km s^{-1}, which is much smaller than 2.5 km s^{-1} in the Hα line. Second, there is an asymmetry of the Ca II line velocity variation between the upward motion phase and the downward motion phase, while such asymmetry is absent in the Hα line velocity variation. The rms velocity of the Ca II line is 0.80 km s^{-1} in the phase of upward motion which is significantly smaller than 1.2 km s^{-1} in the phase of downward motion.

This Ca II line often displays emission reversal in the core as was reported by de la Cruz Rodríguez et al. (2013). These are umbral flashes that were originally discovered in the Ca II H and K lines by Beckers & Tallant (1969). These umbral flashes in the Ca II lines are a consequence of shock wave propagation as confirmed by the construction of synthetic observations by Felipe et al. (2014). In our data, however, we do not see such umbral flashes. The line core was always in absorption with no signature of emission reversals and hence there was no trouble in applying the lambdameter method. We think that the absence of umbral flashes in our data may be because our sunspot was not a normal sunspot comprising an umbra and a penumbra, but a pore without a penumbra. The oscillations in our Ca II line data seem to not be strong enough to appear as umbral flashes.

Figure 6 illustrates the three-minute oscillations in the low/middle chromosphere seen though the Na I D_2 line and the Fe I λ5434 line. The second harmonics are noticeable in the wavelet power spectrum of the Na I line as well, even if the power enhancements are not so strong as those in the Hα line and the Ca II line in Figure 5. The second harmonics are not noticeable in the Fe I line, which is not surprising at all because the Fe I line is formed in the upper photosphere and the low chromosphere.

Figure 7 shows that the second harmonics of the three-minute oscillations are strong in the upper chromosphere and transition region seen through the Mg II, C II, and Si IV emission lines. These harmonics appear as high-frequency extrusions from the three-minute oscillation packets in the wavelet power spectra. The high-frequency extrusions are another manifestation of the nonlinearity that was previously identified by the rapid transition from the downward motion to the upward motion and the subsequent slow transition from the upward motion to downward motion (Tian et al. 2014). In fact, not only the second harmonics (power enhancements at periods of about 1.2–1.5 minutes), but also the third harmonics (power enhancements at periods of 0.6–0.7 minutes) are identified at times $t = 12$ to 15 minutes, especially in the wavelet power spectrum of the Si IV line velocity.

Note that significant power in the 1.5-minute band occurs even at times with low power in the 3-minute band (e.g., Ca II at $t \sim 30$ minutes, Si IV at $t \sim 28$ minutes, Fe I at $t \sim 27$ minutes). There is no trace of shock waves in this power. It represents high-frequency oscillation irrespective of wave-steepening. Its nature and origin are not clear. In the following section, we exclude this kind of feature, and confine our detailed analysis to

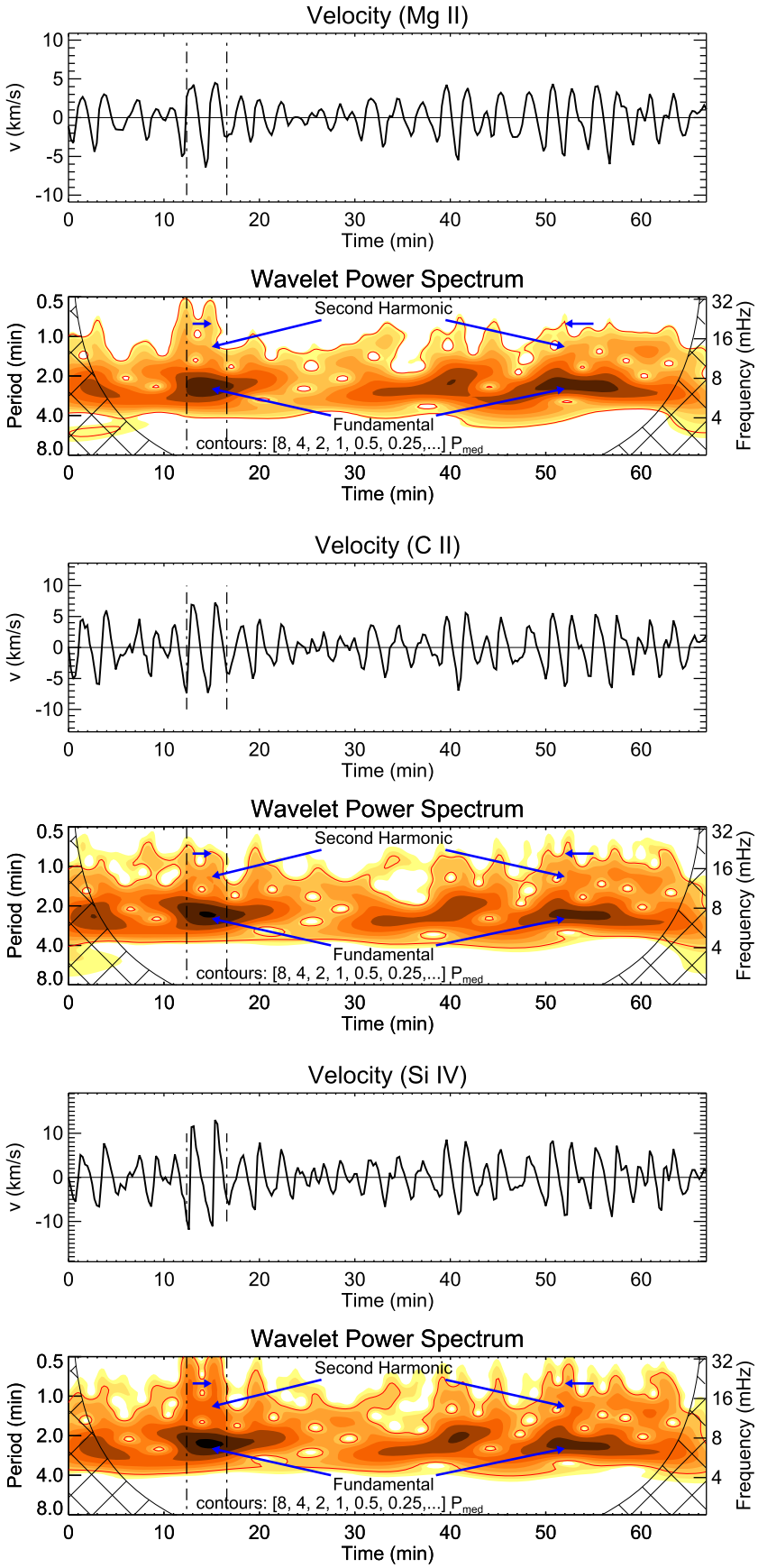

Figure 7. Time series of the Mg II line velocity, its wavelet power spectrum, the time series of the C II line velocity, its wavelet powers spectrum, the time series of the Si IV line, and its wavelet power spectrum (from top to bottom) at the center of a sunspot. The two vertical dotted–dashed lines indicate the temporal span of the data used as an example of the model fit. Each small horizontal arrow indicates the expected occurrence time and period of the third harmonic.

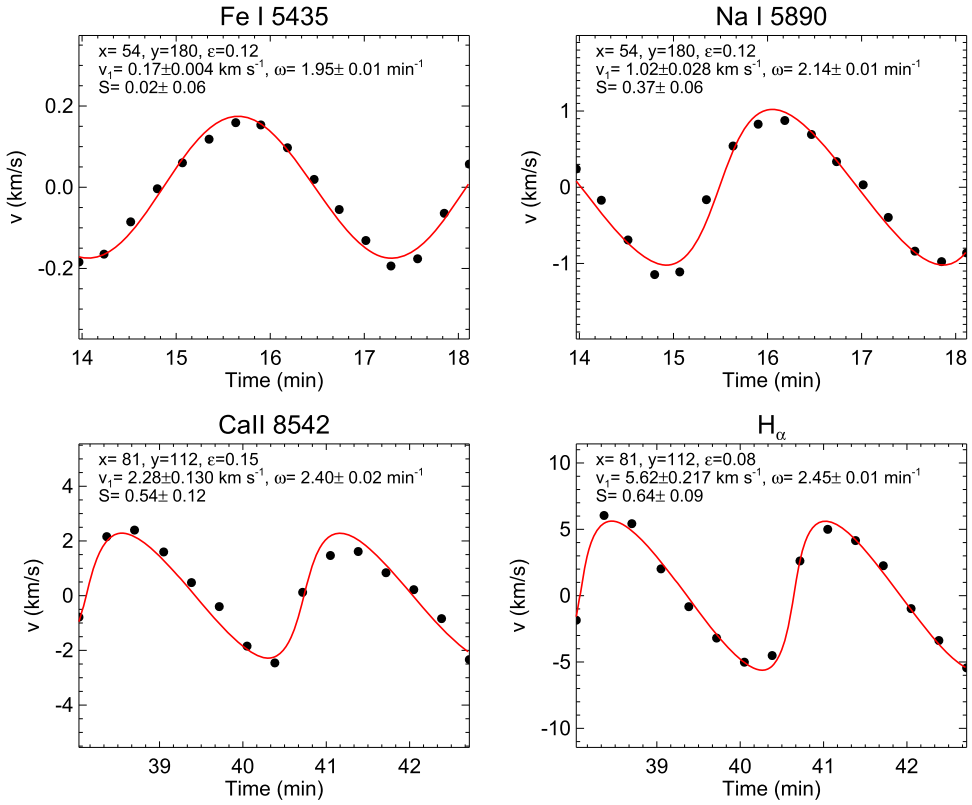

Figure 8. Nonlinear oscillation model fitting of the velocity profile segments of the different lines recorded by the FISS. The Fe I line velocity profile segment and the Na I line velocity profile segment were taken at the same point during the same time interval. The Ca II line profile and the Hα line profile were also taken together at another point.

the temporal spans where both the 1.5-minute band power and the 3-minute band power are strong.

4.2. Nonlinearity Parameters

For the model fitting based on Equation (1), we have selected a number of velocity profile segments that ensure the significantly strong 3-minute power, the constancy of amplitude and period, and a temporal span longer than one wave period. Figure 8 illustrates the model fitting to a velocity profile segment in each line recorded by the FISS. Note that the Fe I velocity profile and the Na I velocity profile were taken from the same location inside a sunspot, corresponding to the temporal spans as indicated in Figure 6. In the same way, the Ca II velocity profile and the Hα velocity were taken from the same location in another sunspot, corresponding to the temporal spans as indicated in Figure 5.

In each plot, we presented the goodness of the fitting as quantified by the fitting error,

$$\epsilon \equiv \frac{\sqrt{\langle (v_{\rm obs} - v)^2 \rangle}}{v_1}, \qquad (10)$$

as well as the determined values of the parameters and their standard error estimates. We find that the model fitting is the best in the velocity data of the Hα line. It is moderately good in the Fe I line data and the Na I line data, and a little poor in the Ca II line data. The coarseness of the fitting in the Ca II line data is related to the abnormal behavior of this line in inferring the velocity, as mentioned above.

Figure 9 illustrates the model fitting to the velocity data of the emission lines recorded by IRIS. These velocity profiles were taken from the same location, and correspond to the temporal spans as indicated in Figure 7. The fitting is fairly good in the C II and Si IV line data, but not good in the Mg II line data. The poor fitting of the Mg II line data may be attributed to the difficulty of inferring the peak velocity of the upward motion due to the contribution of the strong emissions from the highly compressed regions to the line profile, which underestimate the peak velocity. In this specific case, we find that S has comparable values in the Mg II line (0.64) and the C II line (0.60), and a significantly larger value 1.17 in the Si IV line.

Table 2 presents a summary of the model fitting. In each line, 6 to 17 velocity profiles were analyzed for the results. In the cases of the Fe I line, the Na I line, the Hα line, the C II line, and the Si IV line, the fitting is reasonably good, with the mean ϵ being around 0.10. In the case of the Ca II line and the Mg II line, the fitting is a little poor, with ϵ being 0.17. Note that the lines are listed in the table in ascending order of the supposed formation height. This order also becomes the descending order of the main oscillation period P, the ascending order of the velocity amplitude v_1, and the ascending order of S, with a couple of exceptions. The exceptions occur in the Mg II line; the mean values of v_1 and S are not bigger, but are smaller than those of the Hα line. We think these exceptions may be attributed to the underestimated values of v_1 and S of the Mg II line resulting from the poor model fitting of the Mg II velocity profiles.

Figure 10 presents a scatter plot of X and S for all the velocity profiles in the seven spectral lines, as well as the

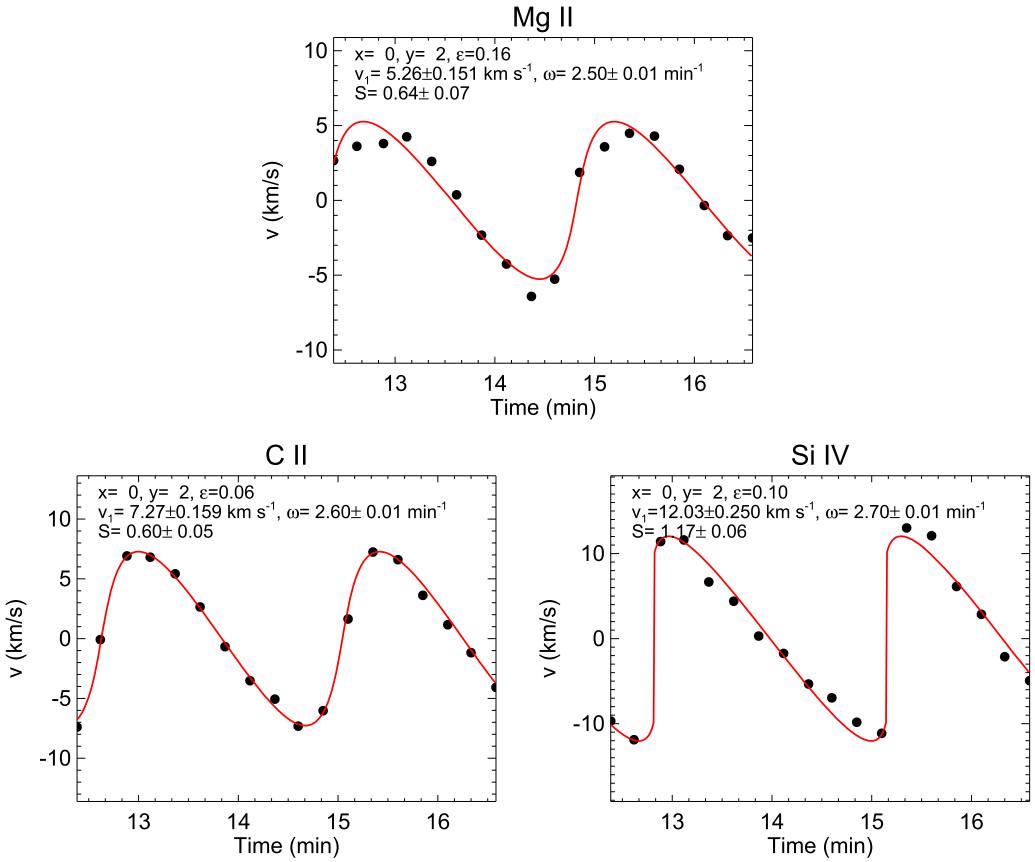

Figure 9. Nonlinear oscillation model fitting of the velocity profiles determined from the different lines recorded by IRIS. All the velocity profiles were taken at the same point.

Table 2
Summary of the Model Parameters (Mean and Standard Deviation) in the Different Lines

Line	N	ϵ	P (minutes)	v_1 (km s^{-1})	log X	S
Fe I 5434	8	0.12	3.02 ± 0.2	0.13 ± 0.03	−1.71 ± 0.07	0.16 ± 0.05
Na I 5890	10	0.11	2.89 ± 0.4	0.74 ± 0.29	−0.96 ± 0.17	0.36 ± 0.06
Ca II 8542	7	0.17	2.77 ± 0.3	1.45 ± 0.44	−0.63 ± 0.17	0.53 ± 0.06
H I 6563 (Hα)	17	0.10	2.61 ± 0.3	3.86 ± 1.01	−0.18 ± 0.13	0.57 ± 0.07
Mg II 2803	7	0.17	2.58 ± 0.4	3.81 ± 1.06	−0.18 ± 0.13	0.43 ± 0.04
C II 1336	6	0.09	2.45 ± 0.2	6.79 ± 1.71	0.09 ± 0.13	0.68 ± 0.04
Si IV 1394	7	0.12	2.38 ± 0.3	8.01 ± 2.32	0.17 ± 0.16	0.84 ± 0.12

Note. N is the number of velocity profiles analyzed in each line.

theoretical curve of S versus X for the three-minute oscillations in an isothermal atmosphere. Note that the theoretical curve is valid for $S < 1$ up to the formation of shock waves. The observations are in agreement with the theory in that they indicate a strong positive correlation between X and S. The best agreement between the observations and theory is found in the data of the Hα line and the Mg II line.

The plot illustrates that the sequence of the Fe I line, the Na I line, the Ca II line, the Hα line/the Mg II line, the C II line, and the Si IV line is the ascending order of formation height, since X is theoretically expected to increase with height. These lines may be categorized into three groups. The first group consists of the Fe I line formed in the low chromosphere, where X is smaller than 0.1. In this group, S is also small, being less than 0.3, and the three-minute oscillations can be considered linear. The second group consists of the Na I line, the Ca II line, and the Hα line, and probably the Mg II line as well, formed in the middle and upper chromosphere, where X is between 0.1 and 1. In this group S is between 0.3 and 0.8. The three-minute oscillations are significantly nonlinear, but the shocks are not fully developed yet. The third group consists of the C II line and the Si IV line formed in the transition region line, where X is bigger than 1. In this group, S is bigger than 0.6. In this group, the three-minute oscillations appear as shock waves.

A comparison of the observational results with the theoretical curve provides us with a basis for the evaluation of

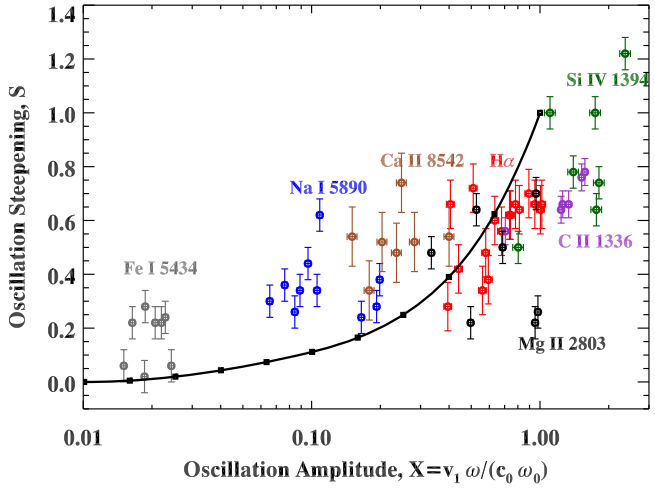

Figure 10. Scatter plot of X vs. S determined from the different spectral lines. The solid curve is the theoretical curve described in Section 2 with $X_0 = 0.01$, and the symbols on the curve correspond to the heights equally spaced between the wave driving height and the shock formation height. The error bars in the data points have been estimated from the model fitting.

velocity inference from each spectral line. In the Fe I line, there exist data points with $S > 0.2$ despite the smallness of X. This is theoretically not expected. More studies are needed to understand this anomaly. In the Na I line, all the data points either have S that are significantly larger or have X that are significantly smaller than theoretical data. A similar behavior occurs in the Ca II line as well. In the Hα line, S seems to be a little underestimated in comparison with theory. In the Mg II line as well, S seems to be underestimated. In fact, the model fitting of the Mg II line data illustrated in Figure 9 suggests that not only S, but also v_1 may be underestimated. In the C II line and the Si IV line, S seems to be underestimated, since theory predicts that the data points with $X > 1$ should have $S > 1$.

5. Discussion

Our study has shown that the nonlinearity of the three-minute oscillations of velocity in the solar atmosphere can be easily identified by the presence of the second harmonic and higher-order harmonics of noticeable power in the wavelet power spectrum of velocity. Moreover, the nonlinearity can be quantified by the two independent parameters: oscillation amplitude X and steepening parameter S that can be measured at different atmospheric levels by analyzing the time series of velocity inferred from the spectral lines formed there. Note that S measures the shape of the velocity profile, and is independent of the magnitude of velocity, while X is directly related to the magnitude of velocity.

We have analyzed the velocity data of sunspots inferred from the seven spectral lines: the Fe I λ5434 line, the Na I D_2 λ5890 line, the Ca II λ8542 line, the Hα line, the Mg II λ2803 line, the C II λ1336 line, and the Si IV λ1394 line, which are listed in the supposed ascending order of the formation height. As a result, we found that the nonlinearity measured by the mean values of either X or S increases with height as theoretically expected. Our results indicate that the three-minute oscillations are linear in the low chromosphere seen through the Fe I line, noticeably nonlinear in the middle chromosphere seen through the Na I line, and highly nonlinear in the upper chromosphere seen through the Ca II line, the Mg II line, and the Hα line, suggesting that the three-minute oscillations form into shock waves in the upper chromosphere. In the transition region seen through the C II line and the Si IV line, the three-minute oscillations seem to appear as well-developed shock waves.

Our results imply that the nonlinearity of the three-minute oscillations can produce higher-frequency oscillations in the upper chromosphere and the transition region. The value of S in these layers is large enough for the second harmonics and third harmonics to have measurable power. It is found that the three-minute oscillations in sunspots have periods ranging from 2.4 to 3.0 minutes. Then, the second harmonic oscillations have periods ranging from 1.2 to 1.5 minutes.

We have shown that the X-S plot is quite useful for comparing the nonlinearity of the three-minute oscillations between observation and theory. We confirm that there is a strong positive correlation between the measured S and X, which is roughly in agreement with theory. Furthermore, in each line a detailed comparison of the data points with theory provides us with the basis for the evaluation of the performance of the velocity inference in the line. The best agreement is seen in the data points of the Hα line, which suggests that the inference of velocity from the Hα line is good, not only for S, but also for X. The big systematic discrepancy between observation and theory is found in the data of the Na I line and the Ca II line. One might attribute this discrepancy to the inadequacy of the assumption of the isothermal atmosphere used for the nonlinear wave solution. We note that the lower part of the real solar atmosphere can be approximated to be isothermal reasonably well. For example, according to the model M umbral atmosphere of Maltby et al. (1986), the atmosphere is fairly isothermal in the layer from 0 to 800 km above the photospheric surface. The formation of the Na I line is very likely to occur within this isothermal part of the atmosphere. Nevertheless, we cannot exclude the possibility that the formation of the Ca II line may occur above this part where temperature increases with height. In this upper part of the chromosphere, not only the non-isothermal structure of the atmosphere, but also the radiative cooling may have to be taken into account in the propagation of nonlinear acoustic waves, as was done in the study of the propagation of linear waves by Centeno et al. (2006) and Bloomfield et al. (2007) using the pair of the photospheric Si I λ10827 line and the chromospheric He I λ10830 line. Further work is needed to see how these factors affect the theoretical relationship between X and S.

From an observational perspective, the discrepancy could be resolved if v_1 or X were multiplied by a factor of about 3 in the Na I line, and by a factor of about 2 in the Ca II line. This suggests that the velocity inferred from these lines using the lambdameter method may have been underestimated by the same factors. This possibility of velocity underestimates in these two lines seems to justify a future investigation.

We conclude that the two independent nonlinearity parameters S and X are measurable and can be used to compare theory and observations in the nonlinear propagation of three-minute oscillations. Further works are definitely needed to remove the discrepancies between theory and observations. For example, from a theoretical standpoint, the solution has to be found for the shock waves (with $S > 1$) propagating in the atmosphere, where the temperature increases with height. From an observational standpoint, the technique of inferring chromospheric velocity from spectral lines has to be elaborated, making use of the non-LTE radiative transfer of the spectral

lines in an atmosphere where three-minute oscillations propagate.

We are grateful to the referee for a number of valuable constructive comments. This work was supported by the National Research Foundation of Korea (NRF-2017 R1A2B4004466). Y.L.'s contribution was supported by the Alexander von Humboldt Foundation and by the Ruhr-Universitat Bochum Graduate School. The BBSO operation is supported by NJIT, US NSF AGS-1250818, and NASA NNX13AG14G, and the GST operation is partly supported by the Korea Astronomy and Space Science Institute and Seoul National University.

ORCID iDs

Jongchul Chae https://orcid.org/0000-0002-7073-868X
Kyuhyoun Cho https://orcid.org/0000-0001-7460-725X
Donguk Song https://orcid.org/0000-0002-7737-740X
Yuri E. Litvinenko https://orcid.org/0000-0002-1845-5877

References

Beckers, J. M., & Schultz, R. B. 1972, SoPh, 27, 61
Beckers, J. M., & Tallant, P. E. 1969, SoPh, 7, 351
Bloomfield, D. S., Lagg, A., & Solanki, S. K. 2007, ApJ, 671, 1005
Centeno, R., Collados, M., & Trujillo Bueno, J. 2006, ApJ, 640, 1153
Chae, J., & Goode, P. R. 2015, ApJ, 808, 118
Chae, J., Lee, J., Cho, K., et al. 2017, ApJ, 836, 18
Chae, J, & Litvinenko, Y. 2017, ApJ, 844, 129
Chae, J., Park, H.-M., Ahn, K., et al. 2013a, SoPh, 288, 1
Chae, J., Park, H.-M., Ahn, K., et al. 2013b, SoPh, 288, 89
Chae, J., Song, D., Seo, M., et al. 2015, ApJL, 805, L21
Chae, J., Yang, H., Park, H., et al. 2014, ApJ, 789, 108
Christopoulou, E. B., Skodras, A., Georgakilas, A. A., & Koutchmy, S. 2003, ApJ, 591, 416
de la Cruz Rodríguez, J., Rouppe van der Voort, L., Socas-Navarro, H., & van Noort, M. 2013, A&A, 556, A115
De Pontieu, B., Hansteen, V. H., Rouppe van der Voort, L., van Noort, M., & Carlsson, M. 2007, ApJ, 655, 624
De Pontieu, B., Title, A. M., Lemen, J. R., et al. 2014, SoPh, 289, 2733
Deubner, F.-L., Waldschik, T., & Steffens, S. 1996, A&A, 307, 936
Felipe, T., Khomenko, E., Collados, M., & Beck, C. 2010, ApJ, 722, 131
Felipe, T., Socas-Navarro, H., & Khomenko, E. 2014, ApJ, 795, 9
Fleck, B., & Schmitz, F. 1991, A&A, 250, 235
Hansteen, V. H., De Pontieu, B., Rouppe van der Voort, L., van Noort, M., & Carlsson, M. 2006, ApJL, 647, L73
Kalkofen, W., Rossi, P., Bodo, G., & Massaglia, S. 1994, A&A, 284, 976
Kentischer, T. J., & Mattig, W. 1995, A&A, 300, 539
Lamb, H. 1909, Proc. London Math. Soc., 7, 122
Lighthill, J. 1978, Waves in Fluids (Cambridge: Cambridge Univ. Press)
Lites, B. W., & Thomas, J. J. 1985, ApJ, 294, 682
Litvinenko, Y., & Chae, J. 2017, A&A, 599, A15
Maltby, P., Avrett, E. H., Carlsson, M., et al. 1986, ApJ, 306, 284
Rouppe van der Voort, L., & de la Cruz Rodriguez, J. 2013, ApJ, 776, 56
Tian, H., DeLuca, E., Reeves, K. K., et al. 2014, ApJ, 786, 137
Torrence, C., & Compo, G. P. 1998, BAMS, 79, 61